DESIGN OF A BENDING MAGNET FOR THE KSTAR NBI SYSTEM

SANG RYUL IN, BYEONG JOO YOON* and BEOM YEOL KIM
Nuclear Fusion Research Lab.,
Korea Atomic Energy Research Institute
150 Deokjin-dong, Yuseong-gu, Daejeon 305-353, Korea
*Corresponding author. E-mail : bjyoon@kaeri.re.kr

Received March 6, 2006
Accepted for Publication June 13, 2006

The design concept of a bending magnet to be installed in the KSTAR NBI system is presented. It is the function of a bending magnet that removes unconverted ions from the main beam stream and produces an 8 MW, 120 keV deuterium neutral beam. In order to determine the proper size and shape of the bending magnet, a parametric study on the B-field pattern was carried out by changing the dimensions of the pole face model. In addition, the detailed trajectories of the dominant ion species produced in the beam line were calculated. The electrical and cooling parameters of the coil assembly were also estimated.

KEYWORDS : NBI, Bending Magnet, KSTAR, Beam Deflection, Beam Expansion, B-ficld, Beam Trajectory

1. INTRODUCTION

The NBI system for the KSTAR tokamak will provide an 8 MW (120 keV) deuterium neutral beam for heating the tokamak plasma [1]. The NBI system has three ion sources, each of which produces a 7.8 MW ion beam. A part of the ion beam is changed into a neutral beam when passing through a gas target, namely the neutralizer. Because a fraction of the neutral beam is also ionized again in the neutralizer, there is a maximum attainable neutralizing efficiency depending on the ion species and the beam energy, regardless of how thick the gas target is [2]. The ion beam unconverted in the neutralizer, which cannot penetrate the magnetic barrier of the tokamak, should be removed from the main beam stream by an ion separation device such as a bending magnet so as not to deposit an excessive heat load on the structures surrounding the beam passage.

The ion species produced in the ion source and the beam passage are three main positive ions, $D^+(E)$, $D^+(E/2)$, $D^+(E/3)$; minor negative ions, $D^-(E)$, $D^-(E/2)$, $D^-(E/3)$; minute molecular ions, $D_2^+(E)$, $D_3^+(E)$, $D_2^+(2E/3)$; and miscellaneous ions from residuals, $O^+(16E/18)$, $H^+(E/18)$, $H^+(E)$, where E denotes the beam energy. Table 1 summarizes the fractions of the residual ion species and the partitioning of the beam power for the 7.8 MW (120 keV) deuterium beam (equivalent to a 60 keV hydrogen beam). The main component is the full energy D^+ ions, but the contribution from the molecular ion species is negligible.

The bending magnet (BM) to be installed in the NBI system will be of a transparent type, which transmits ions at different specified bending angles depending on the mass and the energy of the ion. The major ions deflected in the bending magnet are terminated on the ion dump system, and the minor ones are terminated on the beam scrapers. As the beam energy is increased, the neutral efficiency is lowered and the ion beam power becomes greater. Therefore, the heat load on the ion dump at full power operation of the ion source would be too high to withstand, and some methods to alleviate the heat load should be devised. From this aspect, the bending magnet is the first option for reducing the power load on the ion dump to a level below the allowable limit, namely 10 MW/m^2, by expanding the beam cross-section on the dump plate.

In this paper, a design concept for the BM of the KSTAR NBI system is described. The detailed trajectories

Table 1. Number Fraction and Power Partitioning of the Ion Species

	$D^+(E)$	$D^+(E/2)$	$D^+(E/3)$	$D^-(E)$	$D^-(E/2)$	$D^-(E/3)$	$D_2^+(E)$	$D_2^+(2E/3)$
Number Fraction	0.46	0.056	0.052	3.25E-03	2.61E-03	5.61E-03	2.16E-09	4.30E-09
Power [MW]	3.588	0.2184	0.1352	2.54E-02	1.02E-02	2.19E-02	1.68E-08	2.24E-08

of several dominant ion species produced in the ion source and the beam line are simulated, and the electrical and cooling parameters of the coil assembly of the BM are estimated.

2. ANALYTICAL APPROACH ON THE DEFLECTION OF CHARGED PARTICLES IN AN IDEAL BM

The motion of a charged particle moving in a magnetic field (B-field), with a speed of v (or energy E), charge q, and mass m, is represented by the bending angle $\Delta\theta$, which is obtained as;

$$\frac{d\theta}{dt}=\frac{v}{r}\rightarrow\frac{d\theta}{ds}=\frac{1}{r}=\frac{qB}{mv}\rightarrow$$
$$\int d\theta=\int\frac{q}{mv}Bds\rightarrow\int Bds=\frac{mv}{q}\Delta\theta=\frac{\sqrt{2mE}}{q}\Delta\theta \quad (1)$$

where r is the curvature radius of the bending arc and s is the traveling distance along the beam trajectory. This relation does not depend on the practical B-field distribution. It is defined that $\Delta\theta \square 0$ if $q \square 0$.

Assuming that the BM has a rectangular B-field regime of $W \times L$ in the vertical cross-section, and it is inclined to the beam axis (**x**) by an angle δ (refer to Fig. 1), the required B-field integral B_I, along the pole axis ($\mathbf{x}'$, $\mathbf{x}' = \mathbf{x}$ if $\delta = 0$), which is a basic design parameter of the BM to deflect an ion by $\Delta\theta$, is then given by

$$\int BdW=\int\cos(\delta-\theta)Bds=\frac{\sqrt{2mE}}{q}\int_0^{\Delta\theta}\cos(\delta-\theta)d\theta\equiv B_I \quad (2)$$

This relation is also independent of the B-field pattern. If δ is 0° (vertically erected) or 45° (inclined), Eq. (2) is changed to Eq. (3) or Eq. (4).

$$B_I=\frac{\sqrt{2mE}}{q}\sin\Delta\theta\,, \quad (3)$$

$$B_I=\frac{2\sqrt{mE}}{q}(\sin^2\alpha+\sin\alpha\cdot\cos\alpha) \quad (4)$$

where $\alpha = \Delta\theta/2$. Equations (3) and (4) can be solved for $\Delta\theta$ as follows:

$$\Delta\theta=\sin^{-1}\sqrt{2}K\,, \quad (5)$$

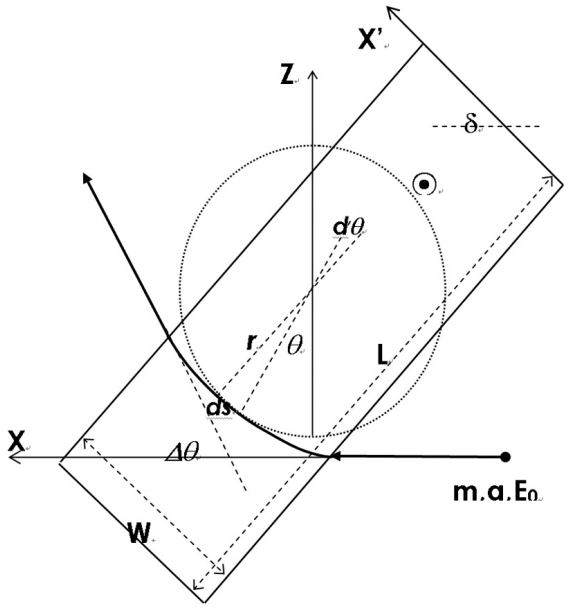

Fig. 1. A Deflection Diagram of Charged Particles in the Magnetic Field

$$\Delta\theta=2\sin^{-1}\left(\frac{\sqrt{1+2K-\sqrt{(1+2K)^2-8K^2}}}{2}\right), \quad (6)$$

where $K\equiv\frac{q\cdot B_I}{2\sqrt{mE}}$, and $\alpha=\frac{\Delta\theta}{2}$.

In the above equations the value of $\Delta\theta$ can remain unchanged by adjusting B_I to maintain K constant for any set of E, m and q. Therefore, the same ion dump system can admit both deuterium and hydrogen ion families of any beam energy.

Figure 2 shows the relationship between $\Delta\theta$ and B_I for 120, 60 and 40 keV D^+ ions in the BM for $\delta = 0°$ and 45°. The erected type is slightly more efficient than the inclined type for deflecting the same ions by the same angle, because the path in the magnetic field of the former is slightly longer. However, the BM in our NBI system is designed as an inclined type where the upper space of the BM can be utilized as an ion dump.

Assuming that a well defined area of the width W is filled with a uniform B-field defined as B_0 so as to clarify the parametric relationship governing the deflection of the charged particles, the bending trajectory forms a part of a circle with the curvature radius given by (refer to Fig. 1)

$$r=\frac{mv}{qB_0}=\frac{\sqrt{2mE}}{qB_0}=\frac{\sqrt{2}W}{1+\sin\Delta\theta-\cos\Delta\theta}\equiv r_{\Delta\theta} \quad (7)$$

From Eq. (7), by defining A □ 70780 G · cm for a 120 keV D^+ ion for example, simple expressions for B_I (= WB_0) to attain desired amounts of $\Delta\theta$ are given as follows:

$$\begin{aligned}
&\text{when} \quad WB_0 < \frac{\sqrt{2}}{4}(\sqrt{3}+1)A\,, \quad \Delta\theta < 60°,\\
&\text{when} \quad \frac{\sqrt{2}}{4}(\sqrt{3}+1)A \le WB_0 < \sqrt{2}A\,, \quad 60° \le \Delta\theta < 90°,\\
&\text{when} \quad \sqrt{2}A \le WB_0 < (1+\frac{1}{\sqrt{2}})A\,, \quad 90° \le \Delta\theta < 135°,\\
&\text{when} \quad (1+\frac{1}{\sqrt{2}})A \le WB_0\,, \quad \Delta\theta = 270°.
\end{aligned} \tag{8}$$

The last term means that any bending angle larger than 135° in the BM inclined by 45° to the beam axis is practically equal to 270°, and the ions at this condition cannot pass through the BM, but rather are reflected.

Table 2 summarizes the values of WB_0 for the D^+ and H^+ ions, and B_0 in a pole gap of width W = 200 mm. While B_0 is different from a real B-field, which has a broad distribution, it is useful for estimating the order of magnitude and establishing a general trend. In the table, $y_{\Delta\theta}$ denotes the amount of vertical movement of a charged particle that has just escaped the BM, and it used to determine the minimum geometrical margin in designing the BM pole face. $y_{\Delta\theta}$ is expressed as

$$\int Bdy = \frac{\sqrt{2mE}}{q}\int_0^{\Delta\theta}\sin\theta d\theta = \frac{\sqrt{2mE}}{q}(1-\cos\theta) \equiv B_0 y_{\Delta\theta}$$

$$y_{\Delta\theta} = r_{\Delta\theta}(1-\cos\Delta\theta) \tag{9}$$

In order to separate the three main ion beam components from each other as clearly as possible, a scheme entailing 60°, 86° and 120° deflection for the ions of full, half, and third energy, respectively, is the most reasonable solution (refer to the gray-colored row in Table 2). These values are chosen because the three components are spread in roughly the same manner at an even angle, and 120° is practically the highest bending angle that can be obtained safely for the third energy component. For example, if the bending angle of a 120 keV ion is greater than 61.17°, that of a 40 keV ion becomes 270°.

A schematic diagram of the BM pole and the major beam trajectories for the above deflection scheme are illustrated in Fig. 3. In the figure the minimum bottom margin to accommodate the lowest path of a full energy ion is $f_b = (1\text{-}1/\sqrt{2})r_{60°} = 2(\sqrt{2}\text{-}1)/(1+\sqrt{3})W \approx 0.3W$; the minimum upper margin to accommodate the uppermost path of a third energy ion is $f_{u1} = \sqrt{2}\, y_{120°}\text{-}W$; and the minimum ideal pole length is $L_{id} = \sqrt{2}H+f_b+f_{u1} = \sqrt{2}(H+y_{120°})+f_b\text{-}W \approx \sqrt{2}H+0.57W$ ($y_{120°} = 1.5r_{120°} = 3\sqrt{2}W/(3+\sqrt{3})$ from Eq. (7)). If the B-field is slightly increased to a value above the desired level, the deflection angle of the third energy ion will be larger than 135°, as noted above. In this worst case, the upper margin

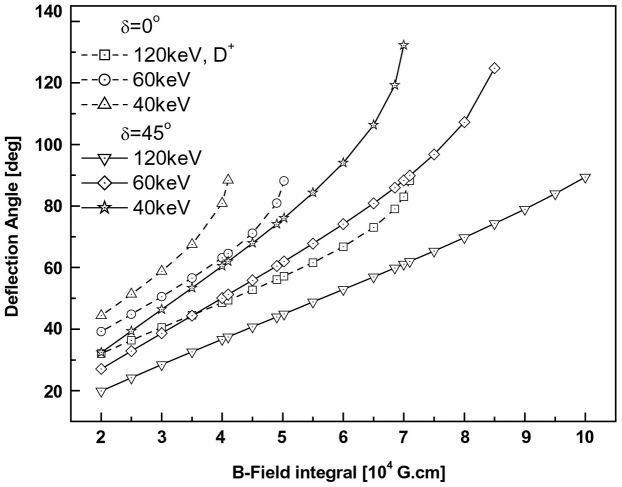

Fig. 2. The Deflection Angle for Three Ion Species as a Function of the Magnetic Field Integral

Table 2. Energy Dependency of the Deflection Angle of the Major Components

$\Delta\theta$ [deg] 120keV	WB_0 [G.cm]		B_0 [G]*		$\Delta\theta$ [deg]		$r_{\Delta\theta}$ [cm]			$y_{\Delta\theta}$ [cm]		
	D^+	H^+	D^+	H^+	60keV	40keV	120keV	60keV	40keV	120keV	60keV	40keV
50	56211	39767	2811	1988	69.6	87	25.2	17.8	14.5	9.0	11.6	14.5
55	62552	44253	3128	2213	77.6	100	22.7	16.0	13.1	9.7	12.6	15.4
60	68601	48532	3430	2427	86.2	120	20.7	14.6	12.0	10.4	13.7	17.9
61.17	69998	49521	3500	2476	88.4	135	20.3	14.3	11.7	10.5	13.9	20.0

* Present values are obtained when W=20 cm

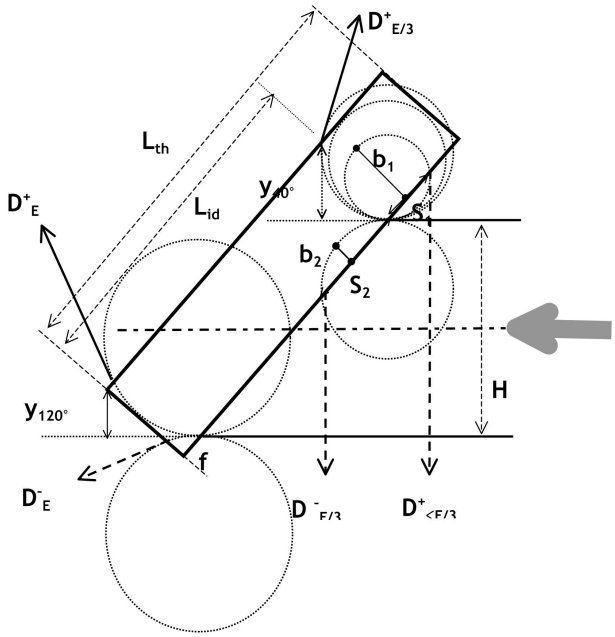

Fig. 3. Simplified Trajectories of Some Ions Passing Through BM Inclined by 45°

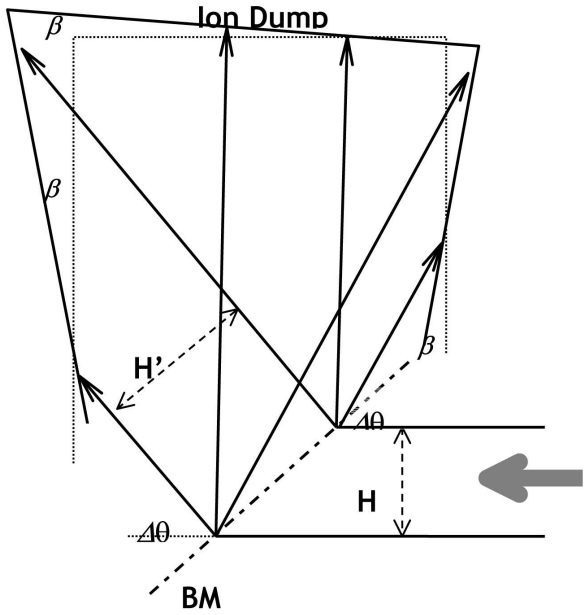

Fig. 4. Projection of Dominant Ions on the Ion Dump Plates

given by $f_{u2} = (1+1/\sqrt{2})r_{135°} = W$ should be taken into account when sizing the BM pole. The theoretical minimum pole length is then $L_{th} = \sqrt{2}H+f_b+f_{u2} \approx \sqrt{2}H+1.3W$.

A positive ion with a very small bending radius (light mass and/or low energy) always has a bending angle of 270°. In this case, the maximum vertical movement of the trajectory from the beam axis plane is $2r_1$, the penetration depth is $b_1 = (1+1/\sqrt{2})r_1$, and the distance between the in and out points is $s_1 = r_1$. Particles negatively charged are deflected by -90° and also move downward. The maximum penetrating depth is $b_2 = (1-1/\sqrt{2})r_2$ and the distance between the in and out points is $s_2 = \sqrt{2}r_2$. It can be reasonably stated that most of the negative ions are reflected at the entrance edge of the pole gap of the BM.

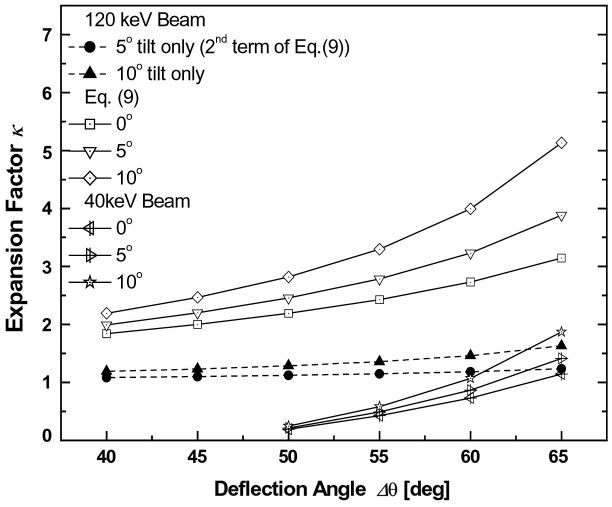

Fig. 5. Variation of the Vertical Beam Expansion Factor vs. the Beam Deflection Angle and the Dump Plate Tilting Angle Note that the Real Deflection Angle of a 40 keV Ion is 180- $\Delta\theta$

3. VERTICAL BEAM EXPANSION

The maximum power density of an ion beam reaching the ion dump is about 50 MW/m^2 at full power operation of the NBI system. The ion beam should be expanded by about 10 times in order to reduce the maximum heat load to far below 10 MW/m^2 for safe operation of the ion dump. There are several methods for mitigating the heat load: 1) natural vertical expansion following a vertical deflection; 2) natural glancing incidence; 3) tilting heat absorbing plates; and 4) horizontal beam expansion.

The resultant vertical expansion factor κ including all the contributions is given by

$$k = \left|1+\tan\Delta\theta\right|\left[\frac{1}{\cos\beta}+\frac{\tan\Delta\theta\cdot\tan\beta}{\cos\beta-\tan\Delta\theta\cdot\sin\beta}\right], \quad (10)$$

$$\Delta\theta \neq 90^{\circ}$$

The first term of Eq. (9) is from the natural expansion during a vertical deflection, expressed as $H'/H = \sqrt{2}\cos(\Delta\theta-\pi/4) = (\cos\Delta\theta+\sin\Delta\theta)$ from Fig. 4. ,which is larger than unity when $\Delta\theta<90°$, and less than unity when $\Delta\theta>90°$, and the term of the glancing incidence on the vertical plate, $1/\cos\Delta\theta$. The second term is from inclination of the plate by β. For a 60 keV ion whose bending angle is nearly 90° and directed to the upper horizontal dump plate, κ is approximately $1/\cos\beta$, ($\approx$1, if β,<<1).

Figure 5 shows the variation of κ as a function of $\Delta\theta$ for the 120 keV and 40 keV ion beams. The effect of tilting the dump plates is small but indispensable to attain the required κ. The 120 keV beam can be expanded by about three times without significant difficulty, but the 60 keV and 40 keV beams at most maintain their original width. Though it is theoretically possible to expand the 120 keV beam by far more than three times, there is a practical limit due to the available vertical space.

An expansion factor of 3 for the 120 keV beam is insufficient and additional expansion is necessary, especially in the horizontal direction. If the magnetic field is uniform in the pole gap, charged particles will only bend on the normal plane to the field lines. However, if there is an axial gradient in the magnetic field, the charged particles may bend additionally on the horizontal plane, as explained in the following section.

4. PRACTICAL B-FIELD DISTRIBUTION AND HORIZONTAL BEAM EXPANSION

A model of the pole face of the BM designed for the KSTAR NBI system is illustrated in Fig. 6. For determining the proper size and shape of the BM, a parametric study on the B-field pattern was carried out, wherein the dimensions of the pole face model were varied. Table 3 shows all the input parameters of the simulations. Fig. 7 shows some typical results of calculations for the distribution of the vertical B-field component B_y, the B-field integral along the pole axis (x′) B_I, in the center plane (y=0), and an example of the field line pattern. The minimum pole gap was fixed at 165 mm to place the pole face as close to the beam aperture of 153 mm as possible. The maximum B-field is influenced by the tapering angle of the pole faces, but not greatly by the pole width. The B-field integral has a larger value for a smaller tapering angle and a wider pole width, because a smaller tapering angle results in a stronger B-field and a wider pole has a broader field distribution. The B-field distribution in the gap on the center plane has a single peak and dull edges, whereas in the plane close to the pole face there may be double peaks, relatively steep edges, and possibly a small negative B-field near the coil assemblies (refer to Fig. 7c and Fig. 8).

The parameter T in Fig. 6 denotes the thickness of the so-called field clamp whose function is to reduce the stray magnetic field outside the pole gap. Figure 8 shows the variation of B_y along the pole axis in the center plane and two edge planes (y=5 mm, 7.5 mm) for three different values of T (25, 50 and 75 mm). No obvious effect of T is found in the B-field distributions on the planes of y=0 and 5 mm. On the plane of y=7.5 mm, a relatively large negative B-field occurs when T=25 mm. A considerable reduction of the negative field is found when the clamp is thickened to 50 mm; however, there is no remarkable improvement when the clamp thickness is increased from 50 mm to 100 mm. The condition of T=75 mm appears to be optimal.

To expand the ion beam in the horizontal plane, the pole gap at the exit is typically designed to be wider than that at the entrance. This artificially generates a negative gradient in the gap, and causes the deflected beam to be first focused and then defocused. However, trajectory calculations using a practically expected B-field pattern show

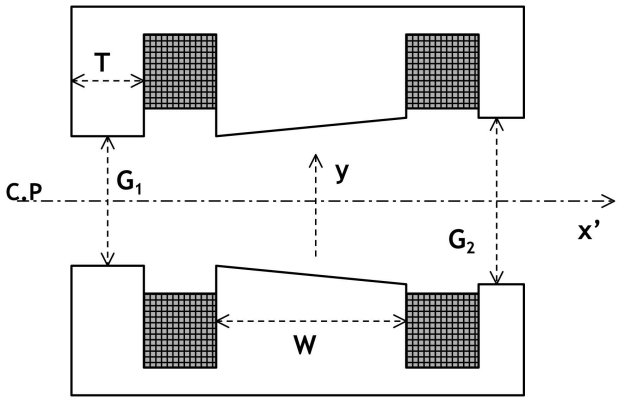

Fig. 6. Cross-section of the BM Pole Face

Table 3. Parameters for the Case Study

	G_1	W	G_2	T	B	NI
1	165	240	165	0	50	20000
2				50	25	
3					50	
4			180			
5			195			
6		300	165			
7		240	205	50		
8		240	205	100		
9		220	200	50		
10		200	195	50		
11		240	205	25		
12		200	190	50		

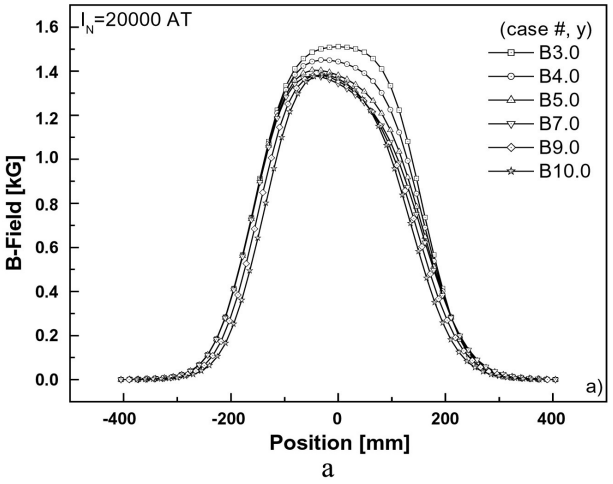

a

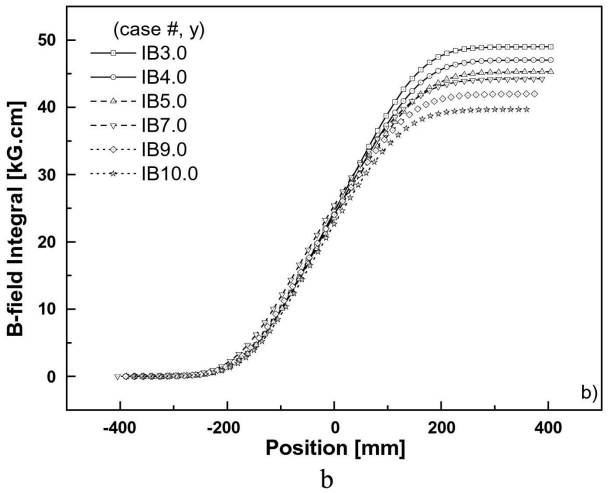

b

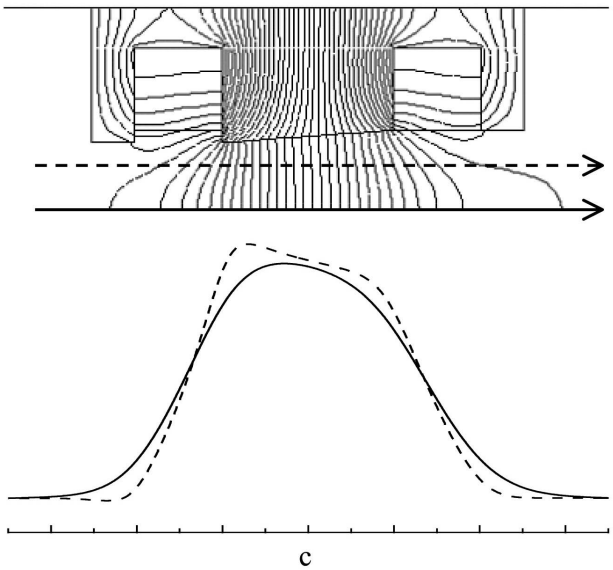

c

Fig. 7. Changes in a) B_y Along the Pole Axis, and b) the B-Field Integral for Several Pole Dimensions. c) the Field Line Pattern of the Final BM Model

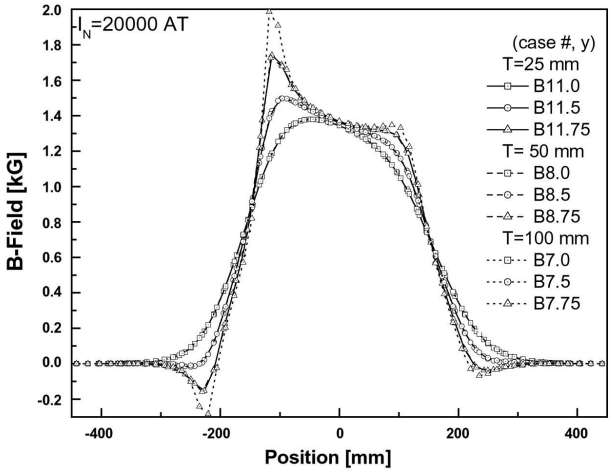

Fig. 8. Comparison of the B_y Distributions on the Center Plane and off the Center Plane

that the beam expands sufficiently even in the BM with parallel pole faces. Figure 9 shows the dependency of the horizontal beam expansion factor and the B-field generation efficiency (B-field integral generated per ampere-turn, B_I / I_N) on the tapering angle of the pole faces. The expansion factor at x=1800 mm (expected position of the full energy dump) is 3.6 even without tapering, which is roughly the target value when β=0. The influence of tapering on the pole face is minor when compared with a natural beam expansion. Moreover, the B-field generation efficiency in the case of the parallel pole faces is greater than that for tapered poles.

The fundamental cause of the natural beam expansion, which occurs in the parallel pole faces, is the field gradient generated around the entrance and the exit of the pole gap. The 45° inclination of the BM enhances the expansion ability, because it generates a cross-field component B_z at the entrance of the BM.

Figure 10 shows the variations of the parameters related to the lateral motion of a 120 keV D^+ ion with a 60° bending angle, projected onto a horizontal plane along a beam path starting from the point (x = 0, y = 50 mm), for the chosen model (refer to the next section). The net inward force acting on the edge beam (y≠0) to the center plane (y=0) is based on the interaction of the axial movement and the positive field gradient, $v_x B_z$, at the entrance of the pole gap, and the interaction of the vertical movement and the negative field gradient, $v_z B_x$, at the exit of the gap. The axial velocity v_x is dominant at the first stage of bending and the vertical velocity v_z becomes dominant after bending by more than 45°. The outward force due to the negative gradient ($v_x B_z$) in the gap is not large enough to reverse the lateral movement, because the absolute value of B_z is very small.

The ion beam, continuously receiving a force directed towards the vertical center plane, consequently forms a

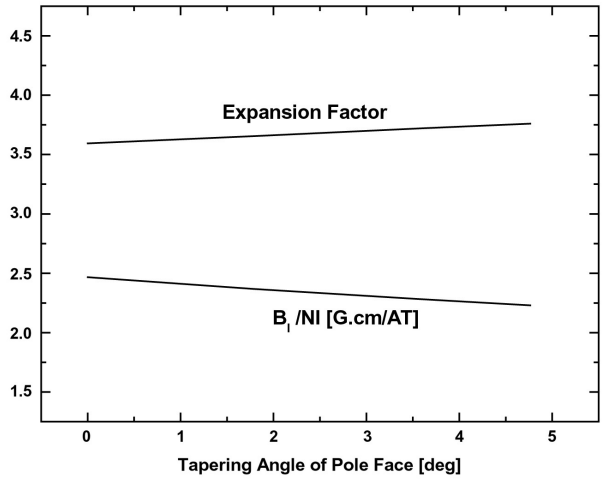

Fig. 9. The Horizontal Expansion Factor and the Specific B-Field Integral as a Function of the Tapering Angle of the Pole Faces

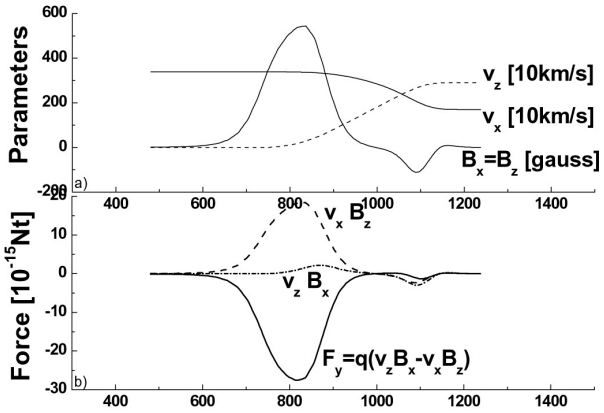

Fig. 10. Variations of the Parameters (velocity terms, B-field terms, force, y-coordinate) Related with the Equation of Motion of Charged Particles

vertical focus line. After focusing, the ion beam crosses the center plane and expands again. If the focal point is formed near the dump, the path length for defocusing will be too short to acquire sufficient horizontal expansion.

5. GEOMETRICAL PARAMETERS OF THE BM AND THE BEAM TRAJECTORY

The ion beam extracted from the last grid of the ion source has an intrinsic divergence depending on the arc plasma properties and the E-field configuration of the grid assembly. The goal of the beam divergence for the ion source of the KSTAR NBI system is 1°. A diagram of the beam power loss at a divergence of 1° is given in Fig. 11. The curve in the figure gives the width of the beam aperture, which contains a certain fraction of the original beam power depending on the distance from the ion source. The narrower the aperture width of the beam line component, the higher the beam loss.

The scrapers of the BM cut the beam loss curve from 14% (upper beam) to 20% (lower beam) depending on their position on the vertical axis. The minimum beam aperture determined by the scraper is 153 mm, and the beam passing through the scrapers diverges by an additional 15 mm or more at the exit boundary of the BM. Therefore, the pole gap at the exit should be larger than 180 mm when taking into account the thickness of the protecting covers of the pole faces, which are usually around 5 mm each. The final design of the BM is such that the pole width is 200 mm, the entrance and exit pole gaps are 165 mm and 195 mm, respectively (refer to case No. 10 in Table 3 and Fig 7). These dimensions are chosen largely on the basis of the minimum clearance required for safety between the pole face and the beam boundary as opposed to enhancing the focusing effect by tapering the pole faces.

Fig. 12 shows the typical trajectories of the dominant ions projected onto the vertical and horizontal planes for the selected BM model. They are calculated by solving an equation of motion for the charged particles in the B-field distribution obtained from the ANSYS code. The direction of the B-field is chosen so that the positive ions move upward to the ion dump located above the head of the BM. Any ions on the vertical center plane move approximately in the same pattern with the analytical cases obtained in section 2, except that they experience larger vertical shifts (for example, +36 mm for 60° bending and +145 mm for 120° bending) due to the broader B-field region. The ions moving near the pole face encounter a B-field having a relatively complicated pattern, as shown in Fig.

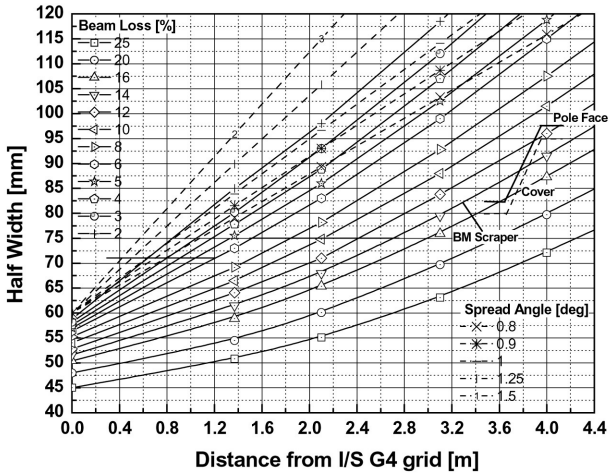

Fig. 11. A Diagram of the Beam Power Loss with the Divergence of 1°

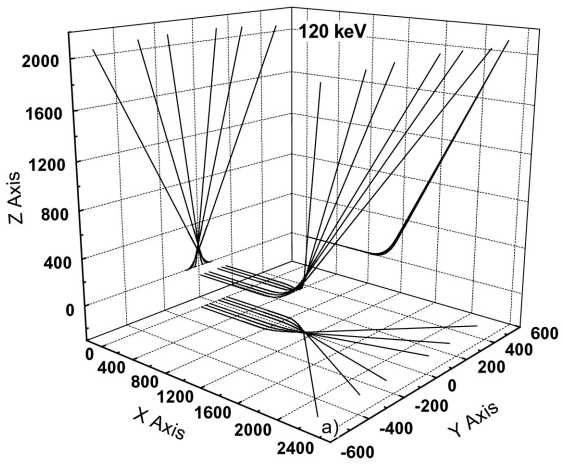

(a)

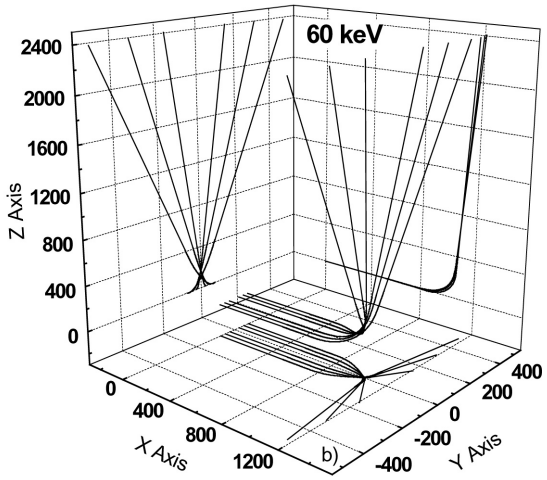

(b)

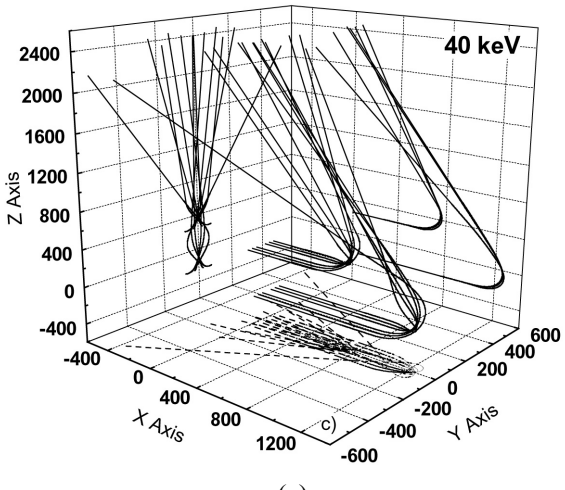

(c)

Fig. 12. Beam Trajectories of the a) 120 kev (center layer), b) 60 keV (center layer), and c) 40 keV (upper and bottom layers) Beam

7c, and their deflection patterns are slightly different from the analytical patterns.

The 40 keV beam, which is much more sensitive to lateral force because of its low energy and travels a relatively long distance in the B-field, experiences repetitive focusing and defocusing on the horizontal plane, while the 120 and 60 keV beams focus only once. The 40 keV ions moving in the upper layer of the beam column may travel over a comparatively short path in the B-field due to the finite size of the BM, and bend by an angle of less than 120°. This results in natural vertical focusing on the ion dump plate.

The negative ions moving near the center plane always bend by -90° and hit the bottom side of the BM including the leg part, while those moving off the center plane are influenced by an outward lateral force and may easily touch the magnet poles before escaping through the pole gap. For reference, there are two methods to safely deflect the negative ions, rotating the magnet by 90° (moving downward) or reversing the direction of the B-field (upward).

Table 4. Deflection Angles of the H^+ & O^+ Ions During a D^+ Extraction

D^+ 120 keV [deg]	H^+ 120 keV	H^+ 60 keV	H^+ 60 keV	$(O^+)_{water}$ 40 keV	$(H^+)_{water}$ 6.7 keV
50	69.6	106.8	270	20.8	270
60 (r=20.7cm)	86.2 (r=14.7cm)	270 (r=10.4cm)	270 (r=8.5cm)	24.8 (r=55cm)	270 (r=3.4cm)

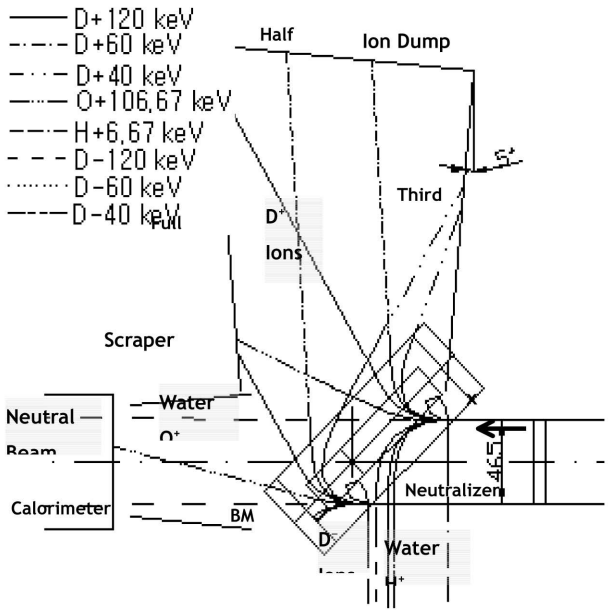

Fig. 13. Major Positive Ions, Minor Negative Ions and Impurity Ions Hitting Beam Stoppers

During D_2 operations there may be some internally originated ions such as H^+ (120 keV) ions from hydrogen residuals in the ion source, H^+ (6.67 keV) and O^+ (106.67 keV) ions from water molecules. In Table 4 the bending angles of such miscellaneous ions are compared with that of the 120 keV D^+ ions. The 120 keV H^+ ions fall exactly on the locations of the 60 keV D^+ ions. The O^+ ions, which are much heavier than hydrogen, deflect by only 25° and deviate from the normal dump location and the regular beam optics. They may hit the region between the ion dump and the calorimeter, and thus may damage any unprotected structures. Moreover, the O^+ beam forms a focusing point too far from the BM to obtain sufficient expansion, and thus the heat load would be intolerable in spite of the relatively small portion of power. The H^+ ions from the water molecules rotate 270°, and the beam may touch the upper leg of the BM if the pole is not sufficiently long.

Figure 13 shows the collective beam trajectories of the ions noted above, moving in the y=0 plane from the exit of the neutralizer to the ion dump plates and the beam scrapers. The tilting angles of the dump plates are all 5°. Even though the ion beam just extracted from the ion source has a rectangular cross-section of a nearly uniform power distribution (144 MW/m^2 for the 7.8 MW beam), the beam gradually diverges when advancing downstream, the power distribution broadens in a bi-Gaussian form, and the peak height lowers. However, the power density at the center of the beam, even after a long traveling distance, is still high enough to instantly damage an insufficiently cooled component. Table 5 summarizes the power load at the hottest point of each dump plate (~5 m downstream from the exit of the ion source), calculated analytically [3]. The values in the parentheses denote the maximum power densities expected when the beam cross-section is maintained at that of original without any artificial expansion except a natural divergence.

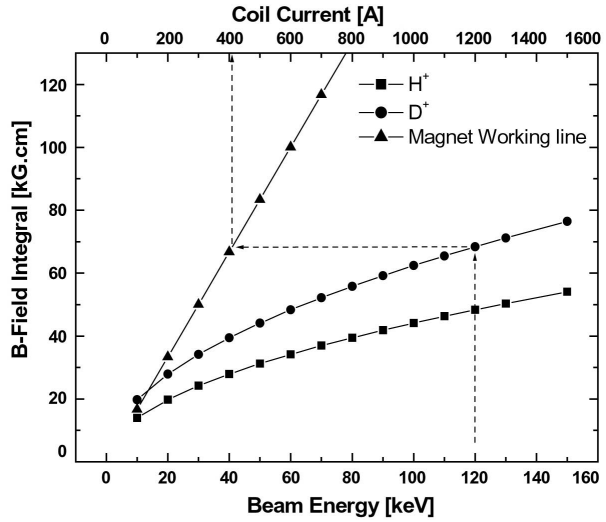

Fig. 14. The Coil Current Demand to Obtain the B-field Integral Required for 60° Bending as a Function of the Beam Energy of H^+ and D^+ ions

Table 5. Maximum Heat Loads on the Ion Dump Plates

	Dump-Full	Dump-Half	Dump-Third
Full Expansion	4	1	2
No Expansion	(47)	(2.7)	(1.8)

6. ELECTRICAL AND COOLING PARAMETERS OF THE COIL ASSEMBLY OF THE BM

The BM will be energized by two encased coil assemblies, one per pole. The coil assembly consists of 2 identical coil modules stacked in a metal case; therefore, the total number of coil modules of the BM is 4. One coil module has 21 turns of a hollow square (12.7mm/ϕ6.5) conductor whose effective conduction area is 128 mm^2, which is practically the thickest conductor available. The coil modules are connected in parallel to cool the water flow. The electrical connection of the coil modules can be a combination of parallel and serial. Different connections require different electrical specifications of the power supply. The current and the voltage of the power supply, and the total power consumption in the coil assembly, are expressed as follows;

$$I = N_p I_c = \frac{I_N}{N_s N_t} \tag{11}$$

$$V = \frac{R_c I_N}{N_p} \tag{12}$$

$$P = IV = \frac{R_c I_N^2}{N_T N_t} \tag{13}$$

where N_p and N_s are the number of parallel and serial coil modules, N_t is the number of winding turns of each coil module, N_T is the total number of coil turns, I_N and I_c are the requirements of the ampere-turns of the BM and the coil current of each module, respectively, and R_c is the resistance of the coil conductor of one module. R_c is expressed as $\rho (N_t l_c + l_d)/A \approx \rho N_t l_c/A$, where ρ is the resistivity of the conductor material, A is the conduction area of the coil conductor, l_c is the length of the coil per turn, and l_t is the length of the extension lead to the power supply. Table 6 compares the variations of the electrical parameters of the coil and the power supply for the three different coil module connections. It is recommended to choose the condition of the last row in the table, as a power supply having an

Table 6. Electrical Parameters of the BM Coil Module and the Power Supply

Width [mm]	Hole Dia. [mm]	Chamfer [mm]	CX Area [mm^2]	Coil Assembly	Modules per Ass.	Turns per Modul.	Total Turns	I_N [AT]	I/turn [A]
12.7	6.5	0.1	128.0984	2	2	21	84	34400	409.5238

Table 7. Examples of the Cooling Calculation

L/turn [m]	L-lead [m]	L/Modul. [m]	Resist. [ohms]	V/Modul. [V]	Parallel	Series	I-BM [A]	V-BM [V]	Q-coil [W]	Q-BM [W]
2.5	10	62.5	0.00839	3.4367	4	1	1638	3.43672	1407.42	5629.67
2.5	10	62.5	0.00839	3.4367	2	2	819	6.87344	1407.42	5629.67
2.5	10	62.5	0.00839	3.4367	1	4	409.5	13.747	1407.42	5629.67

extremely high current is not easily constructed and is therefore expensive.

The working line of the magnet is expressed as 1 A ≡167.5 G · cm. (I_N = 4 ×21I_c = 84I_c = 34400 AT ≡ 68600 G · cm→I_c = 34400÷84 = 409.5 A, 68600÷I_c = 167.5. 34400 AT is the total ampere-turns to obtain the required B-field integral, 68600 G · cm, for bending the 120 keV D^+ ions by 60°.) In Fig. 14 the coil current I_c required to bend the H^+ or D^+ ions by 60° at a certain beam energy can be determined easily.

Regardless of the pattern of the electrical circuit of the magnet coils, each coil module is cooled separately to reduce the pressure drop in the one-pass cooling channel for a required water flow rate. Table 7 summarizes the results of the cooling calculation for the coil module. When the one-pass temperature rise is limited to below 10°C at a power generation of 2.5 kW, the required water flow rate is about 0.06 L/s, the flow speed is 1.8 m/s, and the pressure drop is 1.26 atm.

7. CONCLUSIONS

The present study presents a design concept of a bending magnet to be installed in the KSTAR NBI system to remove ions that are unconverted to neutrals from the main beam stream.

For determining the proper size and shape of the BM a parametric study on the B-field pattern was carried out, wherein the dimensions of the pole face model are varied. The final design of the BM is such that the pole width is 200 mm, and the entrance and exit pole gaps are 165 mm and 195 mm, respectively

The detailed trajectories of several dominant ion species produced in the NBI system were calculated using a practical B-field distribution, and the heat load projected onto the ion dump system was estimated analytically.

Beam expansion of about 10 times is necessary for a full energy beam, and can be realized by a natural vertical expansion, tilting the dump plates, and a horizontal beam expansion in the B-field gradient. The negative ions always touch the wall of the BM, and thus the pole face and bottom leg of the BM must be carefully protected from power loading of negative ions.

The electrical and cooling parameters of the coil assembly were also estimated. The BM has two encased coil assemblies, one per pole, and one coil assembly consists of 2 identical coil modules. One coil module has 21 turns of a hollow square coil conductor. The minimum current and voltage ratings required for the power supply of the BM are 524.3 A and 17.3 V, respectively. The pressure drop of the coil assembly is expected to be 1.26 atm.

REFERENCES

[1] G. S. Lee, et al., Design and construction of the KSTAR tokamak, Nuclear Fusion **41**(10), 1515(2001)

[2] S. R. In and H. J. Shim, Neutral beam evolution in the KSTAR NBI test stand, J. Kor. Vac. Sci. Technol. **7**(1), 1(2003)

[3] L. C. Pittenger, et al., A neutral beam injection system for TFTR, Proc. of 7th Symp. on Eng. Prob. of Fus. Res., 555 (1977)